Reversing Acute Kidney Injury Using Pulsed Focused Ultrasound and MSC Therapy: A Role for HSP-Mediated PI3K/AKT Signaling

Mujib Ullah,[1] Daniel D. Liu,[1] Sravanthi Rai,[1] Arya Dadhania,[1] Sriya Jonnakuti,[1] Waldo Concepcion,[1] and Avnesh S. Thakor[1]

[1]Interventional Regenerative Medicine and Imaging Laboratory, Department of Radiology, Stanford University, Palo Alto, CA, USA

Acute kidney injury (AKI) is characterized by a sudden failure of renal function, but despite increasing worldwide prevalence, current treatments are largely supportive, with no curative therapies. Mesenchymal stromal cell (MSC) therapy has been shown to have a promising regenerative effect in AKI but is limited by the ability of cells to home to damaged tissue. Pulsed focused ultrasound (pFUS), wherein target tissues are sonicated by short bursts of sound waves, has been reported to enhance MSC homing by upregulating local homing signals. However, the exact mechanism by which pFUS enhances MSC therapy remains insufficiently explored. In this study, we studied the effect of bone marrow-derived MSCs (BM-MSCs), in conjunction with pFUS, in a mouse model of cisplatin-induced AKI. Here, BM-MSCs improved kidney function, reduced histological markers of kidney injury, decreased inflammation and apoptosis, and promoted cellular proliferation. Surprisingly, whereas pFUS did not upregulate local cytokine expression or improve BM-MSC homing, it did potentiate the effect of MSC treatment in AKI. Further analysis linked this effect to the upregulation of heat shock protein (HSP)20/HSP40 and subsequent phosphatidylinositol 3-kinase (PI3K)/Akt signaling. In summary, our results suggest that pFUS and BM-MSCs have independent as well as synergistic therapeutic effects in the context of AKI.

INTRODUCTION

Acute kidney injury (AKI) is characterized by a sudden decline in renal function. It is a common complication of conditions, such as chronic hypertension, heart failure, and kidney ischemia, and frequently affects hospitalized patients following surgical procedures or administration of nephrotoxic drugs.[1] In recent years, there has been a substantial increase in hospitalizations for AKI. The Centers for Disease Control and Prevention (CDC) estimates that in the United States, AKI hospitalizations increased from around 1 million in 2000 to nearly 4 million in 2014.[2] Similar trends have been found in other countries, including a 3-fold increase in Denmark[3] and a 13-fold increase in England[4] during similar time frames. AKI is an independent risk factor for end-stage renal disease (ESRD) and death.[5] Moreover, multiple studies have also shown that AKI can trigger the onset of chronic kidney disease (CKD) or exacerbate it when already present.[5–10] Given that there are currently no approved therapies for reversing kidney damage, the standard approach to AKI is mostly supportive in nature: maintaining blood volume through intravenous (i.v.) fluids or diuretics, balancing electrolyte concentrations, and initiating dialysis if necessary. However, even with supportive treatment, AKI is associated with significantly increased morbidity and mortality, with substantially increased costs and hospital stay lengths.[11,12] Thus, there is an unmet need for therapies that can promote the repair and regeneration of injured kidneys and prevent the progression to worsening kidney disease.

Stem cell therapy is a promising approach in regenerative medicine that has been shown to have significant potential for the repair of damaged kidney tissue. Whereas traditional pharmaceutical approaches target only one aspect of the complex pathophysiology of AKI, it has been proposed that stem cells might work through multiple mechanisms to affect tissue repair.[13] Mesenchymal stromal cells (MSCs) have been one of the most popular platforms for stem cell therapy. MSCs are multipotent cells with potent angiogenic and immunomodulatory properties.[14] In animal studies, it has been shown that i.v.-infused bone marrow-derived MSCs (BM-MSCs) home to the kidney and stimulate repair and regeneration following AKI.[15,16] These MSCs exert their therapeutic effects, not by differentiating into new tissue but rather by acting as a mobile reservoir of regenerative molecules.[17] These soluble factors are able to stimulate regeneration through prosurvival, mitogenic, anti-inflammatory, and angiogenic effects, which not only protect surviving kidney cells but also promote their proliferation.[16] Although MSC therapy for AKI has shown promising effects in preclinical settings, many hurdles still limit its efficacy, the most pressing of which is the inefficiency of MSC homing. Since such therapies appear to depend on the paracrine action of MSCs, the proximity of infused MSCs to damaged tissue is thus essential. However, many studies have shown that i.v.-infused
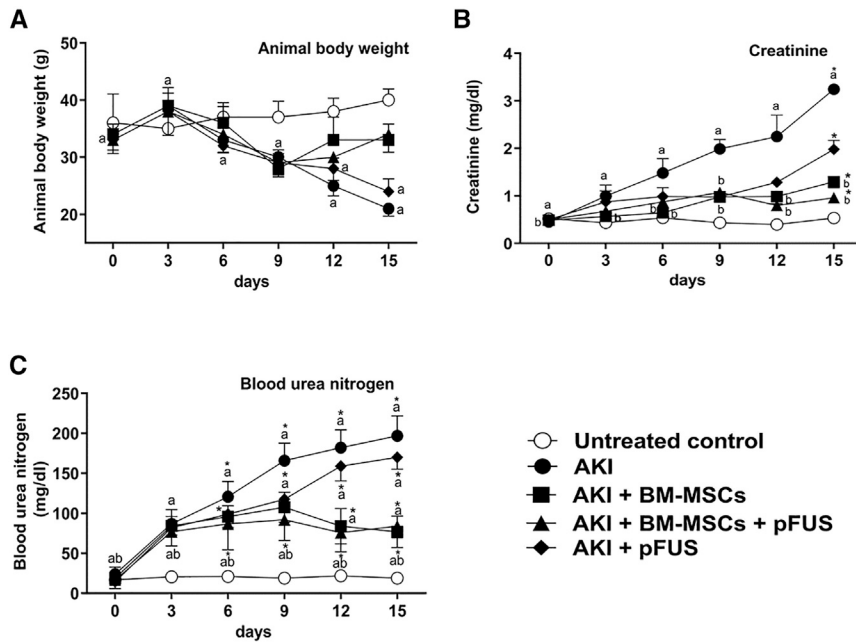
Figure 1. Physical Parameters and Biochemistry of AKI Mice following Cisplatin Injection

(A) Animal body weight. (B) Plasma creatinine levels in animals. (C) Blood urea nitrogen levels in animals. Each group has n = 6, except in AKI, where n = 5. Error bars represent standard deviations. Significant differences include [a]$p < 0.05$ relative to untreated control; [b]$p < 0.05$ relative to AKI; [c]$p < 0.05$ relative to AKI + BM-MSCs; [d]$p < 0.05$ relative to AKI + BM-MSCs + pFUS; *$p < 0.05$ all time points relative to day 0.

BM-MSCs are largely trapped in the lung microvasculature in what is known as the pulmonary first-pass effect.[18–22]

One promising method for improving the homing of MSCs and potentiating their effect is the use of pulsed focused ultrasound (pFUS).[23] pFUS nondestructively sonicates target tissues with short-duration but high-intensity bursts of sound waves, eliciting a range of biological effects. Interestingly, pFUS can promote a transient local increase in cytokines, chemokines, and trophic factors in the sonicated tissue,[24] some of which act as a beacon for circulating MSCs. In keeping with this mechanism, studies have shown that pFUS can enhance MSC homing to sonicated tissues in both healthy murine skeletal muscle[25] and the kidney.[26] Indeed, in a mouse model of cisplatin-induced AKI, pFUS enhanced the therapeutic effect of BM-MSCs (i.e., by improving renal function and mouse survival) by enhancing their homing, permeability, and retention in the damaged kidney.[27] Further studies then suggested that pFUS upregulated interferon (IFN)-γ in the injured kidney, which assists in BM-MSC migration and stimulates BM-MSCs to produce the anti-inflammatory cytokine interleukin (IL)-10.[28]

However, other work has suggested that homing of BM-MSCs to the kidneys may not be necessary for improving kidney repair, as MSCs may act from distant sites via an endocrine mechanism of action, wherein they secrete factors that limit apoptosis and enhance the proliferation of the endogenous tubular cells.[29] Hence, the exact mechanism(s) by which BM-MSCs or pFUS can modulate kidney repair in the setting of AKI are not definitively known. In this study, we therefore induced AKI in mice by administering cisplatin and then examined the effect of BM-MSCs alone, pFUS alone, or combined pFUS + BM-MSC treatment in order to compare the effectiveness

of these three approaches in reversing renal damage and restoring renal function.

RESULTS

Characterization of BM-MSCs

In the present study, we used a pooled sample of BM-MSCs collected from 3 different human donors. These human BM-MSCs exhibited MSC morphology with positive expression of the following surface markers: CD44, CD73, CD90, CD105, and CD166 and negative expression of CD11b, CD24, and CD45 (Figures S1B and S1C). BM-MSCs from passage number 3 (P3) were used for all studies based on their doubling time and colony formation rate (Figures S1D–S1F).

The Biological Effects of BM-MSCs and pFUS in the Setting of AKI

Following administration of cisplatin, there was a significant reduction in body weight in animals in the AKI group compared to untreated controls; however, this effect was ameliorated in those animals that received treatment with either BM-MSCs alone or pFUS + BM-MSCs. pFUS alone did not improve body weight reduction (Figure 1A). By day 3, there was a rise in blood creatinine levels in all animals following cisplatin administration. By day 15, animals in the AKI group showed significantly increased levels of blood creatinine compared to untreated controls (AKI: 3.25 ± 0.08 versus 0.53 ± 0.11 mg/dL, p < 0.05). Treatment with pFUS alone demonstrated decreased blood creatinine levels when compared to AKI group animals, although it did not reach statistical significance (pFUS: 1.98 ± 0.19 versus 3.25 ± 0.08 mg/dL, p > 0.05). In contrast, animals with AKI that were treated with either BM-MSCs alone or combined pFUS + BM-MSCs demonstrated a significant decrease in blood creatinine levels compared to the AKI group (BM-MSCs: 1.30 ± 0.13 versus 3.25 ± 0.08 mg/dL, p < 0.05; pFUS + BM-MSCs: 0.96 ± 0.12 versus 3.25 ± 0.08 mg/dL, p > 0.05) (Figure 1B). Furthermore, at day 3, there was a significant rise in blood urea nitrogen (BUN) levels in all animals treated with cisplatin compared to the untreated control group (AKI: 196.77 ± 35.47 versus 18.79 ± 1.67 mg/dL, p < 0.05). Whereas pFUS alone was able to somewhat decrease BUN compared to the AKI group, it did not reach statistical significance (169.88 ± 7.99 versus 196.77 ± 35.47 mg/dL, p > 0.05).
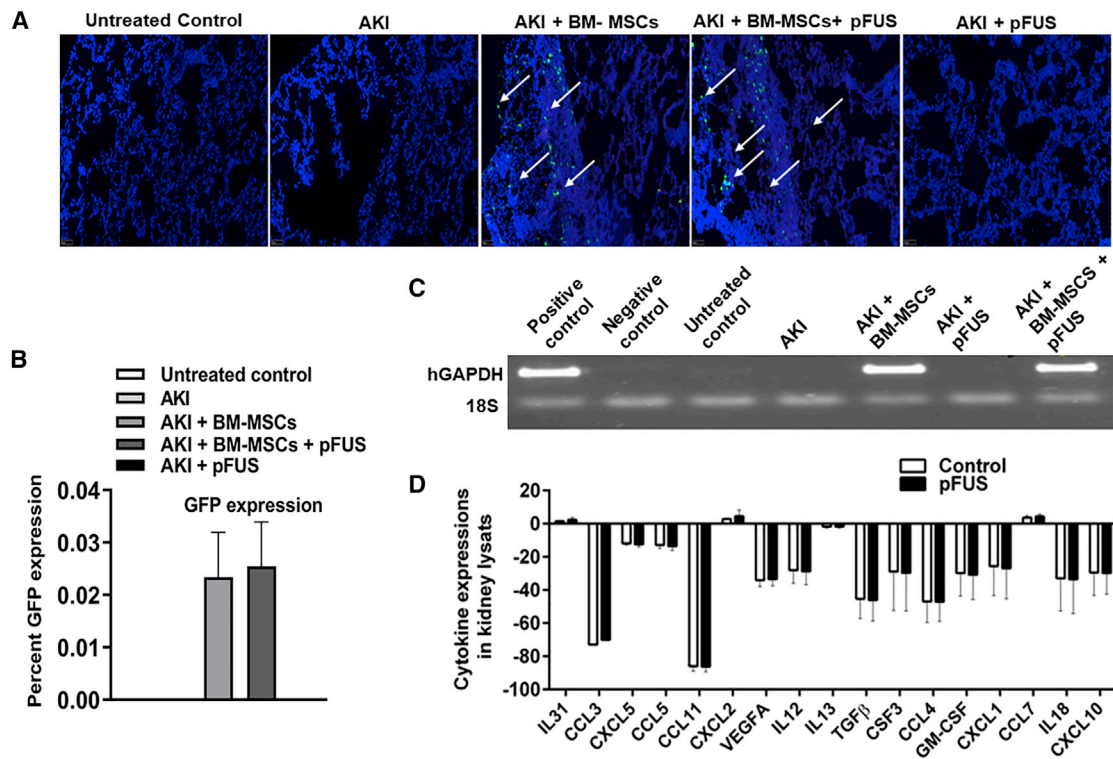
Figure 2. Homing of BM-MSCs

(A) Homing of BM-MSCs, shown by green due to expression of GFP in kidney sections. Each group has n = 6, except AKI, where n = 5 mice, 20 images per animal, was taken. (B) Quantification of GFP signal by flow cytometry in kidney homogenized cells. Each group has n = 6, except in AKI, where n = 5. (C) PCR showing the presence of human GAPDH in treated kidneys. Each group has n = 5 mice. (D) Cytokine expression within kidney lysate samples treated with pFUS, measured 2 days postsonication. Each group has n = 2 mice. Scale bar, 100 μm. Error bars represent standard deviations. Significant differences include [a]p < 0.05 relative to untreated control; [b]p < 0.05 relative to AKI; [c]p < 0.05 relative to AKI + BM-MSCs; [d]p < 0.05 relative to AKI + BM-MSCs + pFUS.

Treatment with BM-MSCs in animals with AKI demonstrated a significant decrease in BUN levels compared to the AKI group (76.77 ± 9.53 versus 196.77 ± 35.47 mg/dL, p < 0.05), and a similar trend was also seen in those animals with AKI treated with pFUS + BM-MSCs (83.77 ± 12.82 versus 196.77 ± 35.47 mg/dL, p < 0.05). However, these values were still significantly higher when compared to untreated control animals (18.79 ± 1.67 mg/dL, p < 0.05) (Figure 1C).

Homing of BM-MSCs to the Kidney in the Setting of AKI

Following the development of AKI in mice, i.v.-administered GFP-labeled BM-MSCs homed to the injured kidney, as detected by immunofluorescence (IF) (Figure 2A), flow cytometry (Figure 2B), and qPCR for human glyceraldehyde 3-phosphate dehydrogenase (GAPDH) (Figure 2C). However, there was no significant increase in the amount of BM-MSCs in the kidney in those animals treated with BM-MSCs + pFUS, as demonstrated by only a minimal increase in the number of GFP-labeled BM-MSCs visible on IF (688 ± 50 versus 710 ± 80 per field, p > 0.05) (Figure 2A), percentage of GFP-positive cells detected on flow cytometry (0.023 ± 0.009 versus 0.025 ± 0.009, p > 0.05) (Figure 2B), and human GAPDH expression by qPCR (Figure 2C). Furthermore, there was no difference in the

cytokine/chemoattractant expression between control kidneys and kidneys treated with pFUS, measured 48 h after sonication (Figure 2D).

Histological and Structural Remodeling of the Acutely Injured Kidney following BM-MSC and pFUS Treatment

Histological evaluation of kidney tissue demonstrated that cisplatin induced a significant increase in indices of kidney injury, such as glomerular casts, tubular casts, and fibrosis, compared to untreated controls (Figures 3A and 3B). When AKI animals were treated with BM-MSCs alone, there was a significant reduction in all of these indices compared to the AKI group (tubular casts: 1.29 ± 0.28 versus 3.88 ± 0.43, p < 0.05; glomerular casts: 1.45 ± 0.42 versus 3.46 ± 0.18, p < 0.05; fibrosis score: 0.88 ± 0.34 versus 3.68 ± 0.44, p < 0.05). Treatment with pFUS alone also yielded some improvement compared to the AKI group (tubular casts: 1.89 ± 0.20 versus 3.88 ± 0.43, p < 0.05; glomerular casts: 2.13 ± 0.31 versus 3.46 ± 0.18, p < 0.05; fibrosis score: 1.65 ± 0.28 versus 3.68 ± 0.44, p < 0.05). However, animals in the combined pFUS + BM-MSC treatment group showed less histological evidence of kidney damage than those in BM-MSC-alone group (tubular casts: 0.98 ± 0.28 versus 1.29 ± 0.28, p > 0.05; glomerular casts: 0.85 ± 0.28 versus
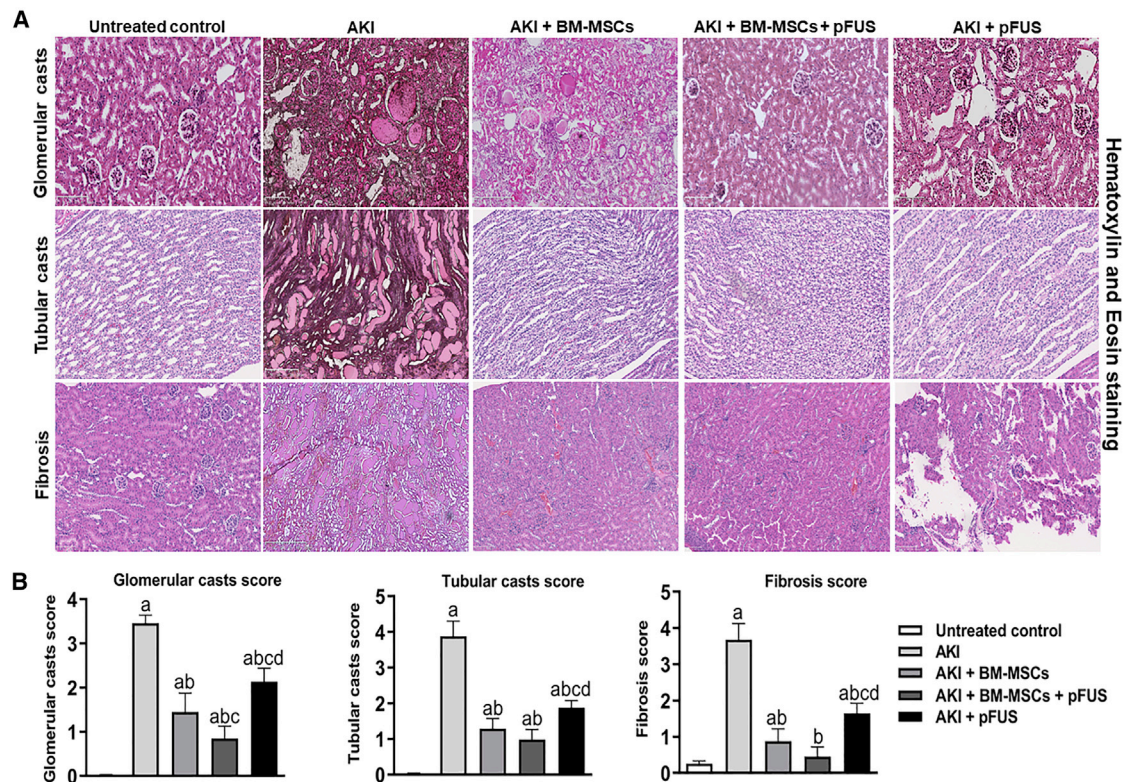
Figure 3. Histological Analysis of Kidneys from Untreated and Treated AKI Mice

(A) Hematoxylin and eosin staining showing the different level of injury, cast formation, and fibrosis across different experimental groups. Scale bars, 100 μm. Each group has n = 6, except AKI, where n = 5, average of 20 images per animal, was taken. (B) Quantification of histological data. Each group has n = 6, except in AKI, where n = 5. Error bars represent standard deviations. Significant differences include [a]p < 0.05 relative to untreated control; [b]p < 0.05 relative to AKI; [c]p < 0.05 relative to AKI + BM-MSCs; [d]p < 0.05 relative to AKI + BM-MSCs + pFUS.

1.45 ± 0.42, p < 0.05; fibrosis score: 0.46 ± 0.26 versus 0.88 ± 0.34, p > 0.05) (Figures 3A and 3B).

Immunohistochemical evaluation of kidney tissue demonstrated that AKI increased the expression of inflammation markers, including tumor necrosis factor-alpha (TNF-α), IL-6, and monocyte chemoattractant protein-1 (MCP-1) (Figure 4A). Whereas treatment of animals with either BM-MSCs alone or pFUS alone reduced the amount of staining of all of these markers compared to the AKI group, the most significant reduction was seen in the group of animals that received treatment with both pFUS + BM-MSCs (Figure 4A).

Similar results were seen when examining the serum levels of these inflammatory cytokines. Our data showed that serum cytokines were significantly increased in animals with AKI compared to untreated controls, both for TNF-α (1,579 ± 189 versus 676 ± 59 pg/mL, p < 0.05) and IL-6 (1,477 ± 92 versus 433 ± 26 pg/mL, p < 0.05) levels. This effect was attenuated when animals with AKI were treated with BM-MSCs alone (TNF-α: 873 ± 100 pg/mL, p < 0.05 and IL-6: 534 ± 39 pg/mL, p < 0.05; Figure 4B) or with both pFUS + BM-MSCs (TNF-α: 558 ± 189 pg/mL, p < 0.05 and IL-6: 587 ± 28 pg/mL, p < 0.05; Figure 4B); in fact, the combined

treatment of BM-MSCs and pFUS resulted in a greater suppression of TNF-α than did either treatment alone. There was no significant change in serum MCP-1 levels across all groups. Both TNF-α and IL-6 demonstrated a similar pattern when their gene expression was assessed at the RNA level by qRT-PCR (Figure 4C). Lactate dehydrogenase (LDH), a marker for renal damage, was significantly upregulated in the kidney for animals with AKI, compared to untreated controls (38.69 ± 3.99 versus 3.30 ± 1.03 relative units, p < 0.05). pFUS alone did not significantly reduce LDH levels compared to the AKI group (28.00 ± 11.00 versus 38.69 ± 3.99 relative units, p > 0.05). However, LDH levels were significantly reduced by both BM-MSCs alone (38.69 ± 3.99 versus 9.00 ± 2.35 relative units, p < 0.05) and the combined pFUS + BM-MSC treatment (38.69 ± 3.99 versus 10.70 ± 2.68 relative units, p < 0.05) (Figure 4D).

The Molecular Effect of BM-MSCs and pFUS on the Kidney in the Setting of AKI

We measured the expression of proapoptotic and anti-apoptotic proteins, including BAX (proapoptotic), B cell lymphoma 2 (Bcl-2; anti-apoptotic), caspase 3 (CASP3; an executioner caspase), and poly [ADP-ribose] polymerase (PARP; contributes to both apoptosis and DNA repair) in all collected kidney samples. Western blot
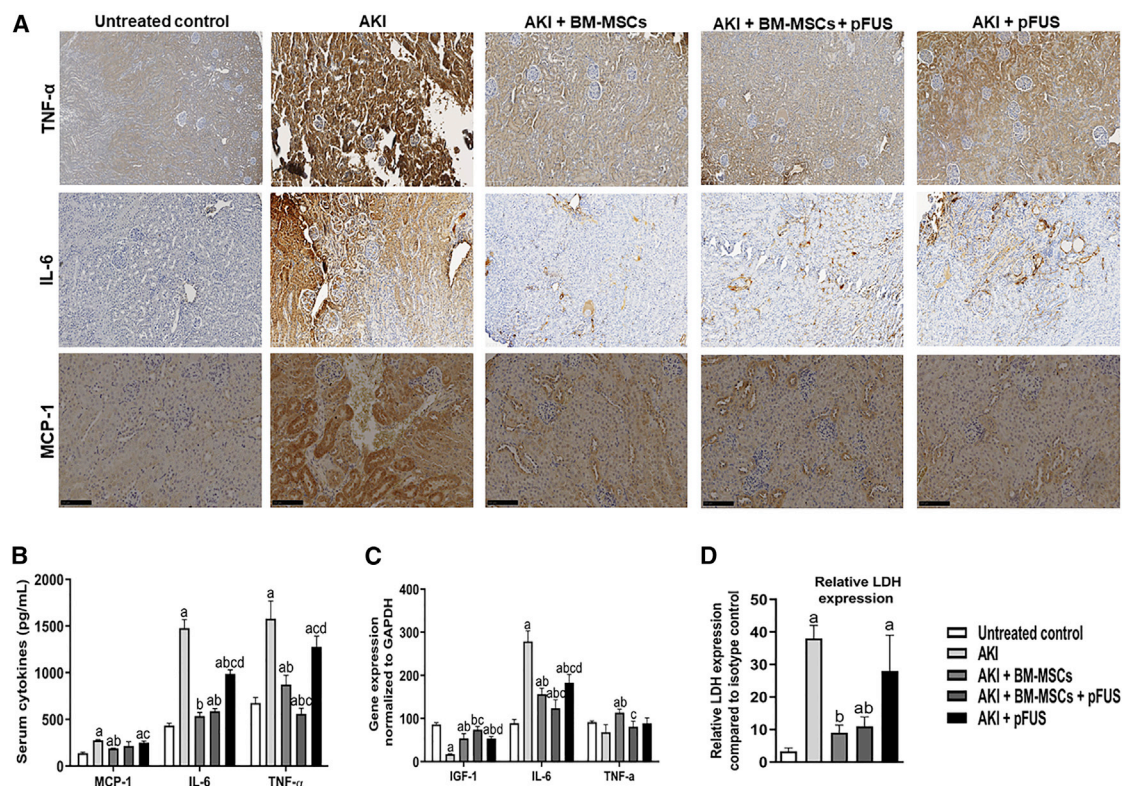
Figure 4. Immunohistochemistry and Assessment of Inflammation in Kidneys from Untreated and Treated AKI Mice

(A) Immunohistochemical staining of inflammatory markers TNF-α, IL-6, and MCP-1 in AKI mice, which are untreated or treated with BM-MSCs alone or BM-MSCs + pFUS.
(B) Serum cytokine measurement of inflammatory markers TNF-α, IL-6, and MCP-1 in AKI mice, which are untreated or treated with BM-MSCs alone or BM-MSCs + pFUS.
(C) qPCR, gene expression of inflammatory markers TNF-α, IL-6, and IGF-1 in AKI mice, which are untreated or treated with BM-MSCs alone or BM-MSCs + pFUS. (D) Relative lactate dehydrogenase (LDH) expression compared to isotype control measured by flow cytometry in AKI mice, which are untreated or treated with BM-MSCs alone or BM-MSCs + pFUS. Scale bars, 100 μm. Each group has n = 6, except in AKI, where n = 5. Error bars represent standard deviations. Significant differences include [a]p < 0.05 relative to untreated control; [b]p < 0.05 relative to AKI; [c]p < 0.05 relative to AKI + BM-MSCs; [d]p < 0.05 relative to AKI + BM-MSCs + pFUS.

analysis revealed cleaved caspase-3 bands in all mice that suffered AKI following cisplatin administration, thereby indicating apoptotic activity (Figure 5A). RT-PCR levels normalized to GAPDH found that Bcl-2 activity was low across all treatment groups (Figure 5B). However, the expression of BAX, PARP, and CASP3 was elevated in animals in the AKI group compared to the untreated control group (BAX: 7.99 ± 1.37 versus 4.99 ± 1.04, p > 0.05; PARP: 6.98 ± 1.20 versus 3.65 ± 0.59, p < 0.05; Bcl-2: 0.45 ± 0.06 versus 0.98 ± 0.31, p > 0.05; CASP3: 2.85 ± 0.10 versus 0.77 ± 1.11, p < 0.05). Treatment with BM-MSCs alone, pFUS alone, and pFUS + MSCs was able to reduce the expression of these proapoptotic genes, often to levels comparable to untreated controls.

We then measured the protein expression of p-ERK1/2 (phosphorylated extracellular signal-regulated kinase 1/2), p-AKT (phosphorylated/activated Akt), and p-AMPK (phosphorylated/activated adenosine 5′ monophosphate-activated protein kinase) in kidney lysates (Figures 5C and 5D). Levels of p-ERK1/2 and p-AMPK were unchanged among all treatment groups. We found that p-AKT was reduced in the AKI group compared to untreated controls

(0.12 ± 0.07 versus 0.99 ± 0.14 arbitrary units, p > 0.05). In animals with AKI, treatment with either BM-MSCs alone or pFUS alone was able to restore p-AKT levels to levels comparable to untreated controls (0.99 ± 0.09 arbitrary units, p < 0.05; 0.77 ± 0.60 arbitrary units, p < 0.05, respectively). The combined pFUS + BM-MSC treatment was also able to increase p-AKT levels compared to AKI, although the change was not statistically significant (0.33 ± 0.09 relative units, p > 0.05).

Next, we evaluated the protein expression of heat shock proteins (HSPs) in all collected kidney samples. In the initial protein array screen, HSP20 and HSP40 were found to be significantly elevated in mice treated with BM-MSCs compared to the AKI group (Figures 6A and 6B). Whereas the level of HSP20 increased only moderately in mice treated with BM-MSCs alone compared to the AKI group (from 24,567 ± 987 to 32,097 ± 4,098 mean pixel density units), this value was greatly increased in those animals treated with both pFUS + BM-MSCs (76,542 ± 9,765 mean pixel density units). For HSP40, the value was significantly increased relative to AKI animals in both the BM-MSC-alone and pFUS + BM-MSC groups (from
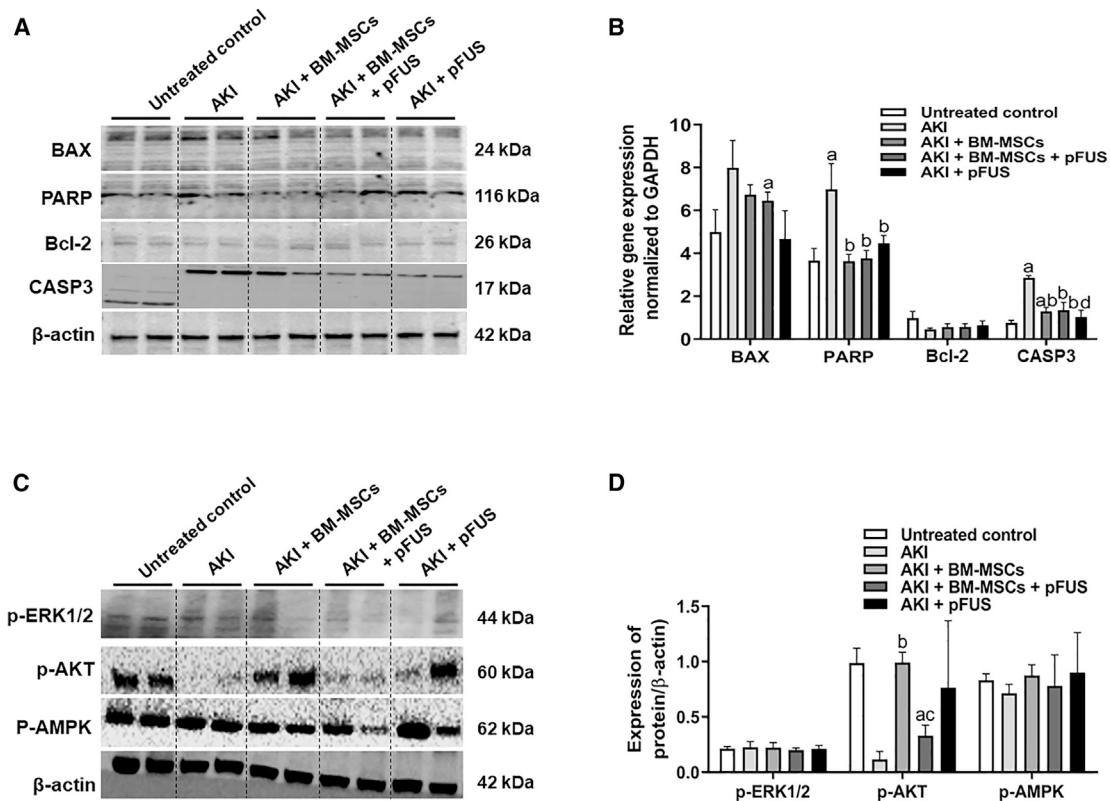
Figure 5. Apoptosis, Cell Death, and Protein Arrays in Kidneys from Untreated and Treated AKI Mice

(A) Western blot showing the expression of BAX, PARP, Bcl-2, CASP3, and β-actin. (B) qPCR showing the expression of BAX, PARP, Bcl-2, and CASP3, normalized to GAPDH. (C) Western blot showing the expression of p-ERK1/2, p-AKT, and p-AMPK (targets of HSP20). (D) Quantification of western blot showing the expression of p-ERK1/2, p-AKT, and p-AMPK (targets of HSP20). Each group has n = 6, except in AKI, where n = 5. Error bars represent standard deviations. Significant differences include [a]$p < 0.05$ relative to untreated control; [b]$p < 0.05$ relative to AKI; [c]$p < 0.05$ relative to AKI + BM-MSCs; [d]$p < 0.05$ relative to AKI + BM-MSCs + pFUS.

$25,098 \pm 10,876$ to $69,872 \pm 5,672$ and $64,351 \pm 9,876$ mean pixel density units, respectively). To validate this significant increase in HSP20 in the AKI animals treated with BM-MSCs and pFUS, we performed western blot analysis and quantification, which confirmed the same pattern (Figure 6C).

The Interaction between HSP20 and HSP40 and Embryonic Kidney Cells

To study the relevance of HSP20 and HSP40, we constructed a small interfering RNA (siRNA) to knock down HSP20 in human embryonic kidney 293 (HEK293) cells. Successful knockdown of HSP20 was confirmed by western blot (Figure 7A). HSP20 knockdown also resulted in a reduction in expression of HSP40 and p-AKT levels (Figures 7A and 7B). These results were further confirmed at the mRNA level via qRT-PCR analysis, which demonstrated a significant decrease in gene expression between HEK293 and HEK293-siRNA groups (HSP20: 5.79 ± 2.19 versus 0.12 ± 0.08, $p < 0.05$; HSP40: 4.03 ± 0.93 versus 0.11 ± 0.01, $p < 0.05$; p-AKT: 1.68 ± 0.20 versus 0.08 ± 0.06, $p < 0.05$) (Figure 7C). Finally, HSP20 knockdown induced cell senescence, as measured by beta-galactosidase (β-Gal) staining (Figure 7D).

When HEK293 cells were treated with pFUS, they expressed increased levels of HSP20 and HSP40, as confirmed by western blot and qRT-PCR (Figures 8A and 8B). This also resulted in an increase in expression in p-AKT levels (Figure 8C).

DISCUSSION

In this study, we have demonstrated that BM-MSCs and pFUS play a role in ameliorating the damage caused by cisplatin-induced AKI. This regeneration was mediated by a reduction of inflammatory cytokines, decreased apoptosis, and increased cell survival and proliferation in the kidney tissue. These effects were shown to be linked to upregulation of HSPs HSP20 and HSP40 and subsequent activation of phosphatidylinositol 3-kinase (PI3K)/Akt signaling, a classical signaling pathway for cell survival and growth. Although combined pFUS + BM-MSC treatment was not consistently superior to the individual treatments in animals with AKI, there were some areas where there was a suggestion of a synergistic effect. For instance, our histological data showed that combined pFUS + BM-MSCs yielded less kidney injury, demonstrated by glomerular casts, tubular casts, and fibrosis, compared to either BM-MSCs alone or pFUS alone. Given the short time course of this study (15 days), this histological evidence
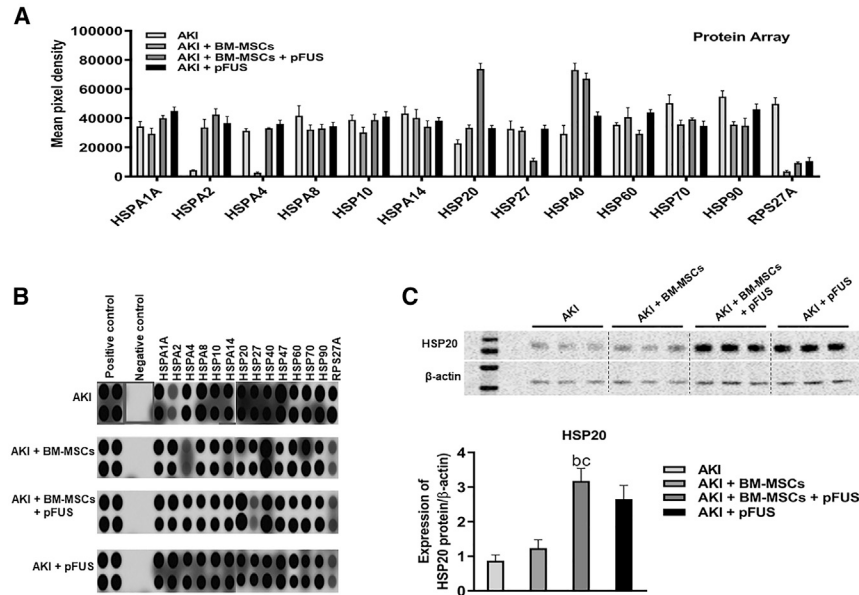
Figure 6. Protein Arrays to Identify the Mechanistic Targets in Kidneys from Untreated and Treated AKI Mice

(A) Quantification of protein arrays showing the comparative expression of various heat shock proteins taken from the protein array data. (B) Blot of protein arrays showing the expression of various heat shock proteins in the form of expression dots in the AKI mice group compared to treatment with BM-MSCs alone or BM-MSCs + pFUS. (C) Validation and quantification of heat shock protein by western blot, showing the expression of HSP20 in the AKI mice group compared to treatment with BM-MSCs alone or BM-MSCs + pFUS. Each group has n = 6, except in AKI, where n = 5. Error bars represent standard deviations. Significant differences include [a]p < 0.05 relative to untreated control; [b]p < 0.05 relative to AKI; [c]p < 0.05 relative to AKI + BM-MSCs; [d]p < 0.05 relative to AKI + BM-MSCs + pFUS.

may be a more important prognostic factor for long-term kidney function than transient inflammatory or apoptosis markers.

Several results in our study differ from previous reports, particularly in three areas: (1) the generation of a cytokine gradient following pFUS, (2) the effect of pFUS on BM-MSC homing, and (3) the therapeutic effect of pFUS alone in the setting of AKI. Ziadloo et al.[26] report that sonication of kidney tissue with pFUS induces a transient increase in cytokines, growth factors, and cell adhesion molecules, lasting for at least 3 days. This local gradient is believed to serve as a beacon to increase BM-MSC homing. Similar to our study, Burks et al.[27,28] tested the effect of pFUS on MSC homing in the context of cisplatin-induced AKI. They report that pFUS increased MSC homing around 1.4-fold and significantly improved renal function and regeneration compared to MSC treatment alone. Furthermore, they reported that pFUS alone had no effect on renal function, apoptosis, or proliferation. However, we observed neither the transient cytokine gradient, 2 days postsonication, nor the resulting increase in MSC homing. Instead, we did observe that pFUS alone has a beneficial therapeutic effect, reducing histological evidence of injury, attenuating inflammation and apoptosis, and promoting proliferation through PI3K/Akt signaling. These discrepancies are probably best explained by differences in sonication parameters; in our study, although we used the same duty cycle, we used a lower pressure (i.e., acoustic energy) of 3 MPa compared to that previously reported at 8.9 MPa. Clearly, different sonication parameters will result in different biological effects,[30] and in the present study, the sonication parameters used appear to upregulate HSPs rather than cytokines and growth factors that facilitate BM-MSC homing. More direct comparisons between our studies and previous literature are made difficult by discrepancies in methodological reporting, making exact replication of sonication parameters difficult.

Instead, our findings suggest that these protective effects may be exerted via protein intermediaries. With the use of western blot and real-time PCR analysis, we found that BM-MSCs and pFUS, both alone and in combination, result in a significant upregulation of HSPs HSP20 and HSP40, as well as activation of PI3K/Akt signaling. In general, HSPs are upregulated in response to stress conditions, whether environmental, metabolic, or pathophysiological.[31] HSP20 (also called HSPB6) is a member of the HSP family, called small HSPs, which acting as ATP-independent molecular chaperones, inhibit or modulate protein aggregation and improve disaggregation processes.[32] Working in conjunction with other HSP families, they thus provide protection against the protein aggregates that could interfere with cellular processes and result in depletion of the factors that are required for protein homeostasis.[33,34] Members of the small HSP family are known to have anti-apoptotic, anti-inflammatory, and proangiogenic properties.[31] HSP20 is known to be expressed in kidney tissue, as well as in the liver, brain, lung, stomach, blood, smooth muscle, skeletal muscle, and cardiac tissue.[35] In addition to kidney injury, increased HSP20 levels are associated with cell protection in MSC transplantation,[36] cardiac ischemia/reperfusion injury,[37] doxorubicin-induced cardiomyopathy,[38] and sepsis-triggered myocardial dysfunction.[39] In the present study, we hypothesize that the increase in HSP20 may play a role in kidney tissue regeneration and repair, which we observed. It is also possible that the increase in HSP40 plays an important role. HSP40 is a downstream target of HSP20, which is known to deliver unfolded or newly synthesized amino acid chains to HSP70, which in turn, assists them in folding into their proper functional forms.[40]

Upregulation of p-AKT is likely another important component of pFUS and MSC therapy, since it is known to be involved in the regeneration and repair processes of damaged kidney tissue.[41,42] PI3K/AKT signaling is a classical pathway for cell proliferation and survival,[43] and there is evidence that it is activated by HSPs, as our knockdown experiments have confirmed. Rat MSCs genetically engineered to
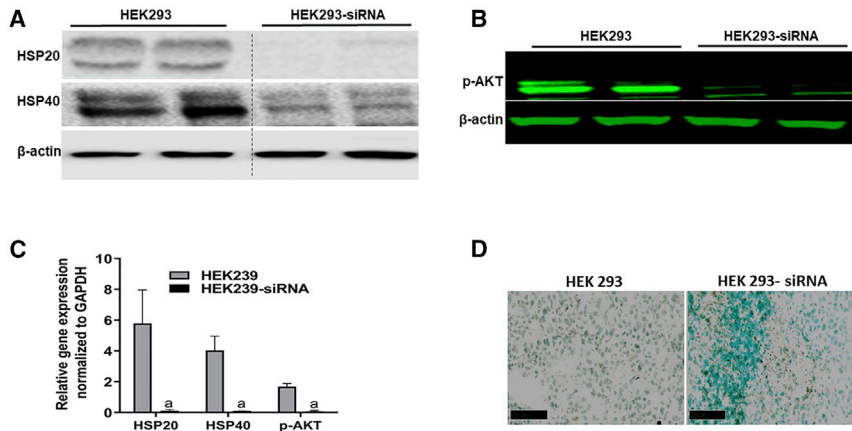
Figure 7. Validation of HSP20 and Its Targets in Cultured Human Embryonic Kidney 293 (HEK293) Cells and HEK293-siRNA HSP20-Knockdown Cells

(A) Western blot of HSP20 and HSP40 in cultured normal HEK293 cells, and HEK293-siRNA HSP20-knockdown cells. (B) Western blot of p-AKT in cultured HEK293 cells and HEK293-siRNA HSP20-knockdown cells. (C) qRT-PCR of HSP20, HSP40, and p-AKT in HEK293 cells and HEK293-siRNA HSP20-knockdown cells. (D) Beta-galactosidase staining, blue showing cell senescence in cultured normal HEK293 cells and HEK293-siRNA HSP20-knockdown cells. Error bars represent standard deviations. Significant difference includes [a]$p < 0.05$ HEK293 versus HEK293-siRNA cells.

overexpress HSP20 demonstrated better survival in response to oxidative stress, both *in vitro* and *in vivo*, and were better able to improve cardiac function in a rat model of myocardial infarction compared to control MSCs; the beneficial effects of HSP20 overexpression were associated with increased Akt phosphorylation and increased secretion of growth factors.[36] HSP20 transgenic mice are also more resistant to doxorubicin-induced cell death, with improved cardiac function and prolonged survival after chronic doxorubicin administration; again, the beneficial effects of HSP20 overexpression appeared to be dependent on direct interaction with p-AKT.[38] Here, we verified the same associations among HSP20, HSP40, and p-AKT *in vitro* that we observed *in vivo*. Given our results, we propose a model of AKI repair whereby HSP20/40 upregulation activates p-AKT, thus regulating anti-apoptotic activity through caspase-3 (considered the most important of the executioner caspases), Bcl-2 (an anti-apoptotic protein), Bax (a proapoptotic protein), and PARP, which plays a dual role in both DNA repair and apoptosis.[44] Activation of caspase-3 and induction of PARP, Bcl-2, and Bax are crucial mediators of programmed cell death.

Another possible repair mechanism is that BM-MSCs counter inflammation by reducing multiple inflammatory cytokines. The significant increases in serum TNF-α and IL-6 that we observed in AKI animals compared to untreated controls were substantially suppressed in animals treated with BM-MSCs alone, pFUS alone, or both. Indeed, the anti-inflammatory effects of BM-MSCs are believed to be major mechanisms by which they protect against renal damage.[45]

Several factors will influence the clinical adoption of BM-MSC and pFUS therapy for treating AKI. On a positive note, there are already Food and Drug Administration (FDA)-approved uses of image-guided therapeutic ultrasound in several areas of medicine, including in the treatment of cardiovascular diseases, tumor ablation, and neurosurgery.[46] In addition, therapeutic ultrasound of the kidneys could be easily carried out at the bedside with the right equipment, easing the adoption of such technologies.[47] Other researchers have noted that there are also pharmacological approaches to increasing

HSP20 that might be considered.[48] For example, both sildenafil and vasoactive intestinal peptide (VIP) have been shown to induce substantial HSP20 phosphorylation in animal models.[49,50] However, these medicinal approaches lack the precision and local targeting made possible by therapeutic ultrasound. Systemic activation of HSP20 and thus, PI3K/AKT signaling may carry the risk of tumorigenesis; indeed, inappropriate PI3K/AKT signaling is associated with many cancers, and there is ongoing research aimed at developing inhibitors of AKT and its downstream target mammalian target of rapamycin (mTOR).[43] With the presumption that additional work confirms our findings, further research would be required to confirm that the positive regenerative effects of HSP20/p-AKT upregulation do not come at the cost of significant safety concerns.

One limitation of this study is that there are many types of cell types within the kidney, and it is unknown which are the exact targets of BM-MSC-mediated regeneration. Our *in vitro* studies on the interaction between HSP20/40 and p-AKT used HEK, but the lineal identity of this cell line is poorly defined.[51] Further *in vivo* studies involving HSP inhibitors and knockout mouse models are thus needed to understand the molecular mechanism through which HSP20 might improve kidney tissue repair and to assess more fully how pFUS and BM-MSCs interact. Thus, whereas we cannot currently make the strong claim that HSP20/40 is directly mediating the therapeutic effect of pFUS and MSCs, our study is the first to link the two, prompting further experiments to elucidate the exact molecular mechanisms. It will also be important to optimize sonication parameters; discrepancies between our studies and previous ones clearly demonstrate that varying the sonication intensity changes the resulting bioeffects. Understanding the relationship between sonication parameters and bioeffects will be essential for determining the best outcomes for clinical translation.

In conclusion, we have shown that both pFUS and BM-MSCs independently result in improved kidney function and regeneration in a mouse model of cisplatin-induced AKI. The beneficial effects appear to be associated with upregulation of HSP20 and p-AKT, reduction of
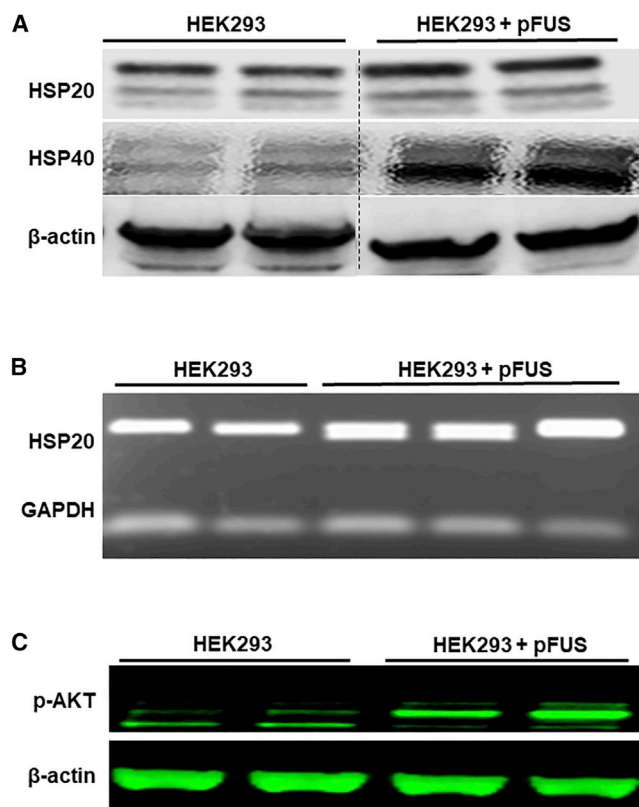
Figure 8. Effects of pFUS on HEK293 Cells

(A) Western blot of HSP20 and HSP40 in cultured HEK293 cells, untreated or induced with pFUS. (B) RT-PCR of HSP20 in cultured HEK293 cells, untreated or induced with pFUS. (C) Western blot of p-AKT in cultured HEK293 cells, untreated or induced with pFUS.

inflammatory cytokines, and increased secretion of growth/regeneration-promoting factors.

MATERIALS AND METHODS

Mice and Animal Models

Eight-week-old female wild-type CD1 mice (34 ± 1.22 g total body weight) were acquired from Charles River Laboratories (Wilmington, MA, USA) and maintained under standard conditions in a pathogen-free facility. Food and water were available to mice throughout the study. Experiments began 2 weeks after animal arrival, and all *in vivo* procedures were carried out according to approved guidelines of the institution's Administrative Panel on Laboratory Animal Care (APLAC). To induce AKI, cisplatin (Sigma-Aldrich, St. Louis, MO, USA) was dissolved in saline and further diluted in phosphate-buffered saline (PBS); this cisplatin mixture (15 mg/kg) was then injected intraperitoneally into mice via a single dose.

To investigate the protective effect of BM-MSCs and pFUS in cisplatin-induced AKI mice, BM-MSCs and pFUS were used either alone or in combination (Figure S1A). Five groups were used in this study: group 1, healthy untreated controls; group 2, AKI, which

received no treatment; group 3, AKI and BM-MSCs alone (i.v. injection of 1×10^6 BM-MSCs via a tail-vein injection); group 4, AKI and pFUS + BM-MSCs, which received pFUS, 4 h before 1×10^6 BM-MSCs i.v.; group 5, AKI and pFUS alone. All treatments were given on day 3 postcisplatin injection, and mice were then observed for another 12 days. At the end of the experimental protocol (day 15), mice were humanely euthanized and their blood, urine, and kidneys collected.

pFUS

A 1.1-MHz central frequency, custom-focused ultrasound therapy transducer (H-102NRE; Sonic Concepts, Bothell, WA, USA) with a 49-mm central opening was used for this study. The ultrasound transducer was then calibrated in a water tank filled with degassed and deionized water. The transducer was driven by an Agilent 33250A function generator (Agilent Technologies, Santa Clara, CA, USA) and connected to a 50-dB ENI 525LA linear power amplifier (ENI Technology, Rochester, NY, USA) and an impedance-matching circuit (Sonic Concepts, Bothell, WA, USA). The transducer was excited at a central 1.1-MHz frequency with 20 cycles at 100 Hz pulse repetition frequency (PRF) in a "burst" mode. A hydrophone (HNR-0500; Onda, Sunnyvale, CA, USA) was placed in the focal spot of the transducer (55 mm away from its surface), and an acoustic intensity measurement system (AIMS III; Onda, Sunnyvale, CA, USA) was used for precise movement and positioning of the hydrophone and digitization of the waveforms. The measured beam profile (full-width, half-maximum area for pressure) at the focal area was 10 mm in length and 1.5 mm in diameter. The intensity and pressure measurements were performed for negative peak pressures (NPPs), up to 3 MPa, in order to reduce risks of hydrophone damage. The transducer was used with the following parameters: 5% duty cycle, 5 Hz PRF, 2.9 MPa NPP, and 272 W/cm^2 spatial average pulse average intensity (I_{sapa}).

For image-guided kidney therapy, a setup of coaligned transducers was used. The imaging transducer (Siemens Acuson S2000 14L5 sp; Siemens, Washington DC, USA) was placed in the central opening of the focused ultrasound transducer. Both transducers were aligned and fixed with a custom-made, 3D-printed holder. The focused ultrasound transducer's focal spot was fixed at 55 mm axial and 0 mm lateral distance from the central point of the imaging transducer. Any misalignment of the focused ultrasound and imaging beam was checked several times in the water tank with the hydrophone and oscilloscope by assembling and disassembling the 3D-printed holder. The measured beam misalignment was less than 200 μm. The ultrasound guidance of the *in vivo* kidney therapy was done using a Siemens S2000 scanner (Siemens Medical Solutions, Issaquah, WA, USA). Mice were kept under anesthesia and submerged vertically in the water tank with their head kept above the water surface. The assembled holder with the focused ultrasound and imaging transducers was then connected to a translation stage and kept in the water at approximately 50 mm axial distance from the mouse. The mouse's kidney was identified on the Siemens S2000 scanner and placed at the desired location, 55 mm axially, 0 mm laterally from the central point

of the imaging transducer. To make treatment uniform, 8 nonoverlapping regions in the kidneys were selected and treated for 30 s each, with a total pFUS therapy time of 4 min for each mouse kidney. The holder was moved from one spot to another using the translation stage so the distance between 2 adjacently treated spots was 2–3 mm.

Cell Culture of the Bone Marrow-Derived Mesenchymal Stromal Cells

Human BM-MSCs were isolated from 3 donors, labeled with GFP (ATCC, USA), grown in culture, and characterized. A frozen vial (1×10^6 MSCs) was thawed at 37°C and plated in complete culture medium consisting of α-minimum essential medium (α-MEM; Gibco, USA), 20% (v/v) fetal bovine serum (FBS; Atlanta Biologicals, USA), 100 U/mL penicillin (Gibco, USA), 100 μg/mL streptomycin (Gibco, USA), and 2 mM L-glutamine (Gibco, USA). After 7 days, the cell layer was washed with PBS, and the adherent viable cells were harvested using 0.25% trypsin and 1 mM EDTA (Gibco, USA) for 5 min at 37°C, reseeded at 1,000 cells per cm^2 in culture medium, and incubated for 7 days until they reached 70%–80% confluence. Cells from passage number 3 were used for all experiments.

Measurements of Creatinine and BUN

Blood samples were collected every 3 days following treatment and at sacrifice. Blood was collected in heparinized tubes and centrifuged at $14,000 \times g$ for 10 min to obtain plasma samples.

Creatinine concentrations were measured using an enzyme-linked immunosorbent assay (ELISA; Stanbio, TX, USA). BUN concentrations were measured using a QuantiChrom Urea Assay Kit (DIUR-500; BioAssay Systems, Hayward, CA, USA).

Histology and Immunohistochemistry

All harvested kidneys were perfused with 4% (v/v) paraformaldehyde in PBS, fixed in formalin for 24 h, and then embedded in paraffin. Samples were then sectioned in 6 μm-thick slices for hematoxylin and eosin and immunohistochemistry. To determine the pathological score, hematoxylin and eosin-stained preparations were evaluated under a light microscope. Dilated tubules, tubular casts, necrosis, and tubular degeneration were scored as described previously.[52] In kidney images, glomeruli and tubular casts and fibrosis were assessed in nonoverlapping fields (up to 20 for each section) using 40 objective images in a single-blind fashion. Glomerular casts and tubular casts were assessed by calculating the percentage of the corresponding structure positive for cast formation. Fibrosis was quantified by calculating the percentage of glomeruli showing evidence of fibrosis. The scoring system used is described as follows: kidneys showing no injury were marked 0, and kidneys exhibiting minimal (<10%), mild (10%–25%), moderate (26%–50%), extensive (51%–75%), and severe (>75%) injuries were assigned scores of 1, 2, 3, 4, and 5, respectively.

For immunohistochemical staining, paraffin-embedded kidney sections were deparaffinized, hydrated, and antigen retrieved; endogenous peroxidase activity was quenched by 3% H_2O_2. Sections were then blocked with 10% normal donkey serum, followed by incubation overnight at 4°C with antibodies, including anti-MCP-1, IL-6, and TNF-α. Next, samples were incubated with secondary antibody for 1 h and then incubated with DAB (3,3-diaminobenzidine) (Vector Laboratories, Burlingame, CA USA). Slides were viewed with a Nikon Eclipse 80i microscope equipped with a digital camera (Nikon, Melville, NY, USA).

Flow Cytometric Analysis

In brief, kidney tissues were cut into small pieces and passed through a 70-μm cell strainer to remove any large pieces. The cell clusters were digested with collagenase dispase (Sigma-Aldrich, St. Louis, MO, USA) at 37°C for 30 min and then dissociated cells filtered (30 μm). The cells were then stained at 4°C in a solution of PBS containing 2% fetal bovine serum. GFP was examined using the fluorescein isothiocyanate (FITC) channel (excitation by blue laser at 488 nm and detection through a 525/550-nm filter). One million cells in 100 μL were incubated for 30 min in the presence of the antibody LDH (Cell Signaling Technology, CA, USA) under saturating conditions (5 μL) and then washed. Analysis was performed using the fluorescence-activated cell sorting (FACS) analysis De Novo software (Glendale, CA, USA).

Cell Culture

HEK293 cells (ATCC, USA) were seeded on 100 cm^2 culture dishes to 60%–70% confluence in complete medium containing 20% FBS for 3 days (culture medium was the same as described above for BM-MSCs). For siRNA knockdown of HSP20, the cells were washed twice with PBS, and then siRNA specific for HSP20 knockdown (OriGene, USA) was added (4 nM) for 24 h. The cells were then harvested and analyzed by western blot and real-time PCR.

Western Blot Analysis

Kidney lysate, cultured BM-MSCs, and HEK cells were lysed in 1 × SDS sample buffer. The kidneys were lysed with radioimmunoprecipitation assay (RIPA) solution containing 1% Nonidet P-40 (NP-40), 0.1% SDS, 100 mg/mL PMSF, 1% protease inhibitor cocktail, and 1% phosphatase I and II inhibitor cocktail (Sigma, St. Louis, Missouri, USA) on ice. The supernatants were collected after centrifugation at $13,000 \times g$ at 4°C for 30 min. Protein concentration was determined by bicinchoninic acid protein assay (Sigma-Aldrich, USA). An equal amount of protein was loaded into a 10% or 15% SDS-PAGE and transferred onto polyvinylidene difluoride membranes. The primary antibodies were as follows: anti-ERK1/2, p-AKT, BAX, BCL-2, HSP20, IL-6, MCP-1, and anti-AMPKα (Cell Signaling Technology, USA); anti-cleaved caspase-3 and PARP (Santa Cruz, USA); and anti-β-actin (catalog sc-1616; Santa Cruz Biotechnology, USA). Quantification was performed by measuring the intensity of the signals with the aid of the NIH ImageJ software package (ImageJ; NIH, USA).

Real-Time PCR

Total RNA was extracted using an RNeasy Mini kit (QIAGEN, CA, USA) and used to synthesize first-strand cDNA by reverse transcription (Applied Biosystems, CA, USA). The quality of cDNA

was assessed by the ratio of the absorbance at 260 and 280 nm. Real-time PCR for mouse insulin growth factor 1 (*IGF1*), *IL6*, *TNFA*, *BAX*, *PARP*, *BCL-2*, *CASP3*, *HSP20*, *HSP40*, and *GAPDH* was performed using TaqMan Gene Expression Assays (Applied Biosystems) and TaqMan Fast Master Mix (Applied Biosystems). All PCR probe sets were purchased from Applied Biosystems. The assays were performed in triplicates for each biological sample. For data analysis, we adopted the $2-\Delta\Delta$ threshold cycle (Ct) method.[53] The Ct of each target gene was first normalized to the Ct of GAPDH in each sample and then to the corresponding value in the control sample.

Senescence-Associated β-Gal (SA-β-Gal) Assay for HEK293 Cells

Cellular senescence was measured by β-galactosidase staining. For assessment of β-galactosidase activity (blue stain positive cells), the cells were fixed with 4% paraformaldehyde for 30 min; washed with PBS; stained with a β-galactosidase detecting kit (Thermo Fisher Scientific, USA), according to the manufacturer's instructions; and examined under a phase-contrast microscope.

ELISA

In brief, we measured the expression level of cytokines in serum obtained from animals belonging to different groups with an ELISA (R&D Systems, CA, USA) using 96-well array plates that were pre-coated with specific cytokine capture antibodies that included MCP-1, IL-6, and TNF-α, as previously described.[54] We then confirmed the concentration of these targets through quantitative PCR.

Statistical Analysis

All data are presented as the mean ± standard deviation (SD). Statistical analysis of the data was performed using Sigma Stat software 4.0 (Systat Software, San Jose, CA, USA) and GraphPad Prism (GraphPad Software, San Diego, CA, USA). Comparison among three or more groups was made using one-way or two-way ANOVA, followed by Tukey's test. Comparison between two groups was made using Student's t test. $p < 0.05$ was considered statistically significant.

SUPPLEMENTAL INFORMATION

Supplemental Information can be found online at https://doi.org/10.1016/j.omtm.2020.03.023.

AUTHOR CONTRIBUTIONS

Conceptualization, M.U., W.C., and A.S.T.; Methodology, M.U. and A.S.T.; Investigation, M.U., D.D.L., S.R., A.D., and S.J.; Writing – Original Draft, M.U., D.D.L., S.R., and A.S.T.; Writing – Review & Editing, M.U., D.D.L., S.R., W.C., and A.S.T.; Funding Acquisition, W.C. and A.S.T.; Supervision, W.C. and A.S.T.

CONFLICTS OF INTEREST

The authors declare no competing interests.

REFERENCES

1. Levey, A.S., and James, M.T. (2017). Acute Kidney Injury. Ann. Intern. Med. *167*, ITC66–ITC80.

2. Pavkov, M.E., Harding, J.L., and Burrows, N.R. (2018). Trends in hospitalizations for acute kidney injury - United States, 2000-2014. MMWR Morb. Mortal. Wkly. Rep. *67*, 289–293.

3. Carlson, N., Hommel, K., Olesen, J.B., Soja, A.M., Vilsbøll, T., Kamper, A.L., Torp-Pedersen, C., and Gislason, G. (2016). Trends in one-year outcomes of dialysis-requiring acute kidney injury in denmark 2005-2012: a population-based nationwide study. PLoS ONE *11*, e0159944.

4. Kolhe, N.V., Muirhead, A.W., Wilkes, S.R., Fluck, R.J., and Taal, M.W. (2015). National trends in acute kidney injury requiring dialysis in England between 1998 and 2013. Kidney Int. *88*, 1161–1169.

5. Coca, S.G., Singanamala, S., and Parikh, C.R. (2012). Chronic kidney disease after acute kidney injury: a systematic review and meta-analysis. Kidney Int. *81*, 442–448.

6. Chawla, L.S., and Kimmel, P.L. (2012). Acute kidney injury and chronic kidney disease: an integrated clinical syndrome. Kidney Int. *82*, 516–524.

7. Chawla, L.S., Eggers, P.W., Star, R.A., and Kimmel, P.L. (2014). Acute kidney injury and chronic kidney disease as interconnected syndromes. N. Engl. J. Med. *371*, 58–66.

8. Pannu, N. (2013). Bidirectional relationships between acute kidney injury and chronic kidney disease. Curr. Opin. Nephrol. Hypertens. *22*, 351–356.

9. Coca, S.G., Cho, K.C., and Hsu, C.Y. (2011). Acute kidney injury in the elderly: predisposition to chronic kidney disease and vice versa. Nephron Clin. Pract. *119* (*Suppl 1*), c19–c24.

10. Hsu, R.K., and Hsu, C.Y. (2016). The Role of Acute Kidney Injury in Chronic Kidney Disease. Semin. Nephrol. *36*, 283–292.

11. Chertow, G.M., Burdick, E., Honour, M., Bonventre, J.V., and Bates, D.W. (2005). Acute kidney injury, mortality, length of stay, and costs in hospitalized patients. J. Am. Soc. Nephrol. *16*, 3365–3370.

12. Leither, M.D., Murphy, D.P., Bicknese, L., Reule, S., Vock, D.M., Ishani, A., Foley, R.N., and Drawz, P.E. (2019). The impact of outpatient acute kidney injury on mortality and chronic kidney disease: a retrospective cohort study. Nephrol. Dial. Transplant. *34*, 493–501.

13. Liu, K.D., and Brakeman, P.R. (2008). Renal repair and recovery. Crit. Care Med. *36* (4, Suppl), S187–S192.

14. Bruno, S., Chiabotto, G., and Camussi, G. (2014). Concise review: different mesenchymal stromal/stem cell populations reside in the adult kidney. Stem Cells Transl. Med. *3*, 1451–1455.

15. Herrera, M.B., Bussolati, B., Bruno, S., Fonsato, V., Romanazzi, G.M., and Camussi, G. (2004). Mesenchymal stem cells contribute to the renal repair of acute tubular epithelial injury. Int. J. Mol. Med. *14*, 1035–1041.

16. Morigi, M., and De Coppi, P. (2014). Cell therapy for kidney injury: different options and mechanisms–mesenchymal and amniotic fluid stem cells. Nephron, Exp. Nephrol. *126*, 59.

17. Caplan, A.I. (2009). Why are MSCs therapeutic? New data: new insight. J. Pathol. *217*, 318–324.

18. Schrepfer, S., Deuse, T., Reichenspurner, H., Fischbein, M.P., Robbins, R.C., and Pelletier, M.P. (2007). Stem cell transplantation: the lung barrier. Transplant. Proc. *39*, 573–576.

19. Santeramo, I., Herrera Perez, Z., Illera, A., Taylor, A., Kenny, S., Murray, P., Wilm, B., and Gretz, N. (2017). Human kidney-derived cells ameliorate acute kidney injury without engrafting into renal tissue. Stem Cells Transl. Med. *6*, 1373–1384.

20. Leibacher, J., and Henschler, R. (2016). Biodistribution, migration and homing of systemically applied mesenchymal stem/stromal cells. Stem Cell Res. Ther. 7, 7.

21. Eggenhofer, E., Benseler, V., Kroemer, A., Popp, F.C., Geissler, E.K., Schlitt, H.J., Baan, C.C., Dahlke, M.H., and Hoogduijn, M.J. (2012). Mesenchymal stem cells are short-lived and do not migrate beyond the lungs after intravenous infusion. Front. Immunol. 3, 297.

22. Fischer, U.M., Harting, M.T., Jimenez, F., Monzon-Posadas, W.O., Xue, H., Savitz, S.I., Laine, G.A., and Cox, C.S., Jr. (2009). Pulmonary passage is a major obstacle for intravenous stem cell delivery: the pulmonary first-pass effect. Stem Cells Dev. 18, 683–692.

23. Liu, D.D., Ullah, M., Concepcion, W., Dahl, J.J., and Thakor, A.S. (2020). The role of ultrasound in enhancing mesenchymal stromal cell-based therapies. Stem Cells Translational Medicine. https://doi.org/10.1002/sctm.19-0391.

24. Burks, S.R., Ziadloo, A., Hancock, H.A., Chaudhry, A., Dean, D.D., Lewis, B.K., Frenkel, V., and Frank, J.A. (2011). Investigation of cellular and molecular responses to pulsed focused ultrasound in a mouse model. PLoS ONE 6, e24730.

25. Burks, S.R., Ziadloo, A., Kim, S.J., Nguyen, B.A., and Frank, J.A. (2013). Noninvasive pulsed focused ultrasound allows spatiotemporal control of targeted homing for multiple stem cell types in murine skeletal muscle and the magnitude of cell homing can be increased through repeated applications. Stem Cells 31, 2551–2560.

26. Ziadloo, A., Burks, S.R., Gold, E.M., Lewis, B.K., Chaudhry, A., Merino, M.J., Frenkel, V., and Frank, J.A. (2012). Enhanced homing permeability and retention of bone marrow stromal cells by noninvasive pulsed focused ultrasound. Stem Cells 30, 1216–1227.

27. Burks, S.R., Nguyen, B.A., Tebebi, P.A., Kim, S.J., Bresler, M.N., Ziadloo, A., Street, J.M., Yuen, P.S., Star, R.A., and Frank, J.A. (2015). Pulsed focused ultrasound pretreatment improves mesenchymal stromal cell efficacy in preventing and rescuing established acute kidney injury in mice. Stem Cells 33, 1241–1253.

28. Burks, S.R., Nagle, M.E., Bresler, M.N., Kim, S.J., Star, R.A., and Frank, J.A. (2018). Mesenchymal stromal cell potency to treat acute kidney injury increased by ultrasound-activated interferon-γ/interleukin-10 axis. J. Cell. Mol. Med. 22, 6015–6025.

29. Bi, B., Schmitt, R., Israilova, M., Nishio, H., and Cantley, L.G. (2007). Stromal cells protect against acute tubular injury via an endocrine effect. J. Am. Soc. Nephrol. 18, 2486–2496.

30. Izadifar, Z., Babyn, P., and Chapman, D. (2017). Mechanical and biological effects of ultrasound: a review of present knowledge. Ultrasound Med. Biol. 43, 1085–1104.

31. Bakthisaran, R., Tangirala, R., and Rao, ChM. (2015). Small heat shock proteins: Role in cellular functions and pathology. Biochim. Biophys. Acta 1854, 291–319.

32. Haslbeck, M., Weinkauf, S., and Buchner, J. (2019). Small heat shock proteins: Simplicity meets complexity. J. Biol. Chem. 294, 2121–2132.

33. Mogk, A., Bukau, B., and Kampinga, H.H. (2018). Cellular Handling of Protein Aggregates by Disaggregation Machines. Mol. Cell 69, 214–226.

34. Haslbeck, M., and Vierling, E. (2015). A first line of stress defense: small heat shock proteins and their function in protein homeostasis. J. Mol. Biol. 427, 1537–1548.

35. Fan, G.C., Chu, G., and Kranias, E.G. (2005). Hsp20 and its cardioprotection. Trends Cardiovasc. Med. 15, 138–141.

36. Wang, X., Zhao, T., Huang, W., Wang, T., Qian, J., Xu, M., Kranias, E.G., Wang, Y., and Fan, G.C. (2009). Hsp20-engineered mesenchymal stem cells are resistant to oxidative stress via enhanced activation of Akt and increased secretion of growth factors. Stem Cells 27, 3021–3031.

37. Fan, G.C., Ren, X., Qian, J., Yuan, Q., Nicolaou, P., Wang, Y., Jones, W.K., Chu, G., and Kranias, E.G. (2005). Novel cardioprotective role of a small heat-shock protein, Hsp20, against ischemia/reperfusion injury. Circulation 111, 1792–1799.

38. Fan, G.C., Zhou, X., Wang, X., Song, G., Qian, J., Nicolaou, P., Chen, G., Ren, X., and Kranias, E.G. (2008). Heat shock protein 20 interacting with phosphorylated Akt reduces doxorubicin-triggered oxidative stress and cardiotoxicity. Circ. Res. 103, 1270–1279.

39. Wang, X., Zingarelli, B., O'Connor, M., Zhang, P., Adeyemo, A., Kranias, E.G., Wang, Y., and Fan, G.C. (2009). Overexpression of Hsp20 prevents endotoxin-induced myocardial dysfunction and apoptosis via inhibition of NF-kappaB activation. J. Mol. Cell. Cardiol. 47, 382–390.

40. Fan, C.Y., Lee, S., and Cyr, D.M. (2003). Mechanisms for regulation of Hsp70 function by Hsp40. Cell Stress Chaperones 8, 309–316.

41. Lan, A., and Du, J. (2015). Potential role of Akt signaling in chronic kidney disease. Nephrol. Dial. Transplant. 30, 385–394.

42. Zhang, G., Wang, Q., Zhou, Q., Wang, R., Xu, M., Wang, H., Wang, L., Wilcox, C.S., Liu, R., and Lai, E.Y. (2016). Protective effect of tempol on acute kidney injury through PI3K/Akt/Nrf2 signaling pathway. Kidney Blood Press. Res. 41, 129–138.

43. Manning, B.D., and Toker, A. (2017). AKT/PKB Signaling: Navigating the Network. Cell 169, 381–405.

44. Elmore, S. (2007). Apoptosis: a review of programmed cell death. Toxicol. Pathol. 35, 495–516.

45. Morigi, M., Rota, C., and Remuzzi, G. (2016). Mesenchymal Stem Cells in Kidney Repair. Methods Mol. Biol. 1416, 89–107.

46. Cleary, K., and Peters, T.M. (2010). Image-guided interventions: technology review and clinical applications. Annu. Rev. Biomed. Eng. 12, 119–142.

47. Chari, S., Nguyen, A., and Saxe, J. (2018). Stem cells in the clinic. Cell Stem Cell 22, 781–782.

48. Fan, G.C., and Kranias, E.G. (2011). Small heat shock protein 20 (HspB6) in cardiac hypertrophy and failure. J. Mol. Cell. Cardiol. 51, 574–577.

49. Gilmont, R.R., Somara, S., and Bitar, K.N. (2008). VIP induces PKA-mediated rapid and sustained phosphorylation of HSP20. Biochem. Biophys. Res. Commun. 375, 552–556.

50. Tessier, D.J., Komalavilas, P., McLemore, E., Thresher, J., and Brophy, C.M. (2004). Sildenafil-induced vasorelaxation is associated with increases in the phosphorylation of the heat shock-related protein 20 (HSP20). J. Surg. Res. 118, 21–25.

51. Lin, Y.C., Boone, M., Meuris, L., Lemmens, I., Van Roy, N., Soete, A., Reumers, J., Moisse, M., Plaisance, S., Drmanac, R., et al. (2014). Genome dynamics of the human embryonic kidney 293 lineage in response to cell biology manipulations. Nat. Commun. 5, 4767.

52. Han, S.J., Li, H., Kim, M., Shlomchik, M.J., and Lee, H.T. (2018). Kidney proximal tubular TLR9 exacerbates ischemic acute kidney injury. J. Immunol. 201, 1073–1085.

53. Ullah, M., and Sun, Z. (2019). Klotho Deficiency Accelerates Stem Cells Aging by Impairing Telomerase Activity. J. Gerontol. A Biol. Sci. Med. Sci. 74, 1396–1407.

54. Amsen, D., de Visser, K.E., and Town, T. (2009). Approaches to determine expression of inflammatory cytokines. Methods Mol. Biol. 511, 107–142.